Yan *et al. Discover Oncology* (2025) 16:1094
https://doi.org/10.1007/s12672-025-02965-7

Discover Oncology

ANALYSIS Open Access

RNA m^{6}A methylation patterns in hepatocellular carcinoma and their association with characteristics of the tumor microenvironment and prognosis

Zongcai Yan[1], Meiling He[1], Lifeng He[2], Liuxia Wei[3] and Yumei Zhang[1*]

*Correspondence:
Yumei Zhang
zhangyumei@gxmu.edu.cn
[1]Department of Medical Oncology, Guangxi Medical University Cancer Hospital, No. 71 Hedi Road, Nanning 530021, Guangxi, People's Republic of China
[2]Department of Thoracic Surgery, The People's Hospital of Guangxi Zhuang Autonomous Region, Nanning 530000, Guangxi, People's Republic of China
[3]Department of Oncology, Ruikang Hospital Affiliated to Guangxi University of Chinese Medicine, Nanning 530011, Guangxi, People's Republic of China

Abstract

Background Methylation at the N^6 atom of adenosine (m^{6}A) of RNA has been linked to immune responses to various types of tumors. How m^{6}A methylation affects tumorigenicity, progression, and tumor microenvironment in hepatocellular carcinoma (HCC) is unclear.

Methods Consensus clustering was used to define m^{6}A methylation patterns based on expression of 26 regulatory factors in HCC. The relative abundance of various immune cell types in the tumor microenvironment was quantified using single-sample gene set enrichment analysis. Cox regression with LASSO was used to screen for genes whose expression correlated with survival of patients with HCC.

Results Two patterns of m^{6}A methylation in HCC were identified: pattern C1 was associated with abundant tumor infiltration by activated CD8$^+$ T cells and by effector memory CD8$^+$ T cells, as well as longer survival; pattern C2 was associated with abundant tumor infiltration by activated CD4$^+$ T cells and by type 2 helper T cells, as well as with shorter survival. Cox regression identified a seven-gene signature capable of predicting the characteristics of the tumor microenvironment and overall survival in HCC: patients in the high-risk group had a lower immunophenoscore, higher TIDE score, and worse survival.

Conclusions Patterns of m^{6}A methylation in HCC are related to immune cell characteristics of the tumor microenvironment and to disease progression and prognosis. Analyzing these patterns in detail may clarify when and how the HCC responds to checkpoint inhibitors and guide the personalization of immunotherapy.

Keywords Hepatocellular carcinoma, m^{6}A modification, Tumor microenvironment, Prognosis, Immunotherapy

1 Introduction

Methylation of RNA at the N^1 or N^6 atom on adenosine or the N^5 atom on cytosine plays a vital role in regulating gene expression [1]. The most common type of RNA methylation in eukaryotic mRNA is at the N^6 atom on adenosine (m^6A), which may influence characteristics of various cancers [2–4]. Alterations in the expression or activity in proteins that catalyze, recognize or remove the m^6A modification [5, 6] may influence gene expression and thereby numerous cellular processes and physiological functions [2, 6, 7], in turn affecting the development and progression of malignant tumors as well as the host's immune responses to them [8–11]. Comprehensive analysis of mutations in m^6A regulators and of their expression may help characterize the heterogeneous tumor microenvironment and identify potential targets for personalized cancer immunotherapy.

Hepatocellular carcinoma (HCC) is the fourth leading cause of cancer-related deaths around the world [12], and its incidence and mortality rate remain high despite widespread vaccination of children against the hepatitis B virus, which is a major risk factor for the disease [13, 14]. Immunotherapies targeting the tumor microenvironment (TME) in HCC are actively being explored. The TME comprises cancer cells on one hand as well as stromal and immune cells on the other [15], and crosstalk between the cancer cells and infiltrating immune cells establish an environment that promotes tumor growth, invasion, and metastasis [16]. Inhibiting the immune checkpoints CTLA-4 and PD-1/PD-L1 [17] in the TME has been explored against HCC, but this strategy failed to meet primary endpoints in the CheckMate-459 and KEYNOTE-240 trials [18], in contrast to its promising performance against other types of cancer [19–21], Moreover, only a small percentage of patients respond to immunotherapy.

Response to tumor immunotherapy may be influenced by m^6A modification [11, 22]. Clarifying how this modification affects infiltration of the TME by immune cells may help predict response to existing immune checkpoint inhibitors and guide the development of novel immunotherapies [23]. Towards this end, the present study analyzed the expression of 26 m^6A regulatory factors in 779 HCC patients from several databases using unsupervised consensus clustering, and it searched for correlations between expression and TME infiltration by immune cells. Two m^6A modification patterns were identified, each associated with a different immune cell profile in the TME. Based on these patterns, a gene signature was constructed that showed promise for predicting overall survival of HCC patients. These findings contribute to understanding how m^6A regulators affect the immune cell characteristics of the TME.

2 Methods

2.1 Collection and preprocessing of data from public datasets

The flowchart of our work is shown in Figure S1. This study made use of publicly available data from the National Center for Biotechnology Information GEO database (www.ncbi.nlm.nih.gov/geo), International Cancer Genome Consortium (ICGC; https://icgc.org), and The Cancer Genome Atlas (TCGA; https://portal.gdc.cancer.gov). Patients with no survival data were excluded from the analysis. The final analysis involved 779 HCC patients from four cohorts: GSE76427 [24] (115 HCC specimens) and GSE116174 (64 HCC specimens) in the GEO database, ICGC-LIRI-JP [25, 26] (232 specimens) and

TCGA-LIHC (368 specimens). The integrated dataset comprising these four cohorts is referred to in the text below and in figures as the "four-cohort HCC dataset".

For the two GSE cohorts, series matrix files and supplementary files, including clinical features and survival data, were downloaded from the GEO database. High-throughput Illumina sequencing data for the GSE76427 cohort were normalized using the RSN method in the "lumi" R package [27], while data for the GSE116174 cohort were processed using the "affy" R package and the RMA algorithm for background adjustment [28].

For the ICGC-LIRI-JP cohort, RNA sequencing data in terms of fragments per kilobase of transcript per million mapped reads (FPKM) as well as data on somatic mutations and clinical information were downloaded. FPKM data were converted to transcripts per kilobase million (TPM) values, which facilitate comparisons across samples and with microarray data [29].

For the TCGA-LIHC cohort, RNA sequencing data in terms of FPKM as well as VarScan-processed somatic mutation data [30] and copy number variations were downloaded. The corresponding data on clinical features and survival were extracted *via* the University of California Santa Cruz (UCSC) Xena browser (https://xenabrowser.net).

Batch effects among the various datasets were removed using the *removeBatchEffect* function in the "limma" R package [31]. Due to the limited availability of normal liver samples in the TCGA, gene expression differences between tumor and normal tissues were explored using a dataset (in TPM format) combining the TCGA cohort and data from the "Therapeutically applicable research to generate effective treatments" (TARGET) dataset and "Genotype-tissue expression" (GTEx) dataset in the UCSC Xena database [32]. The immunotherapy dataset IMvigor210 was downloaded from http://research-pub.gene.com/IMvigor210CoreBiologies [33], and count values were transformed into TPM values. Values of the stemness index of messenger RNA (mRNAsi), which describes how similar tumor cells are to stem cells based on mRNA expression levels, were calculated as described [34].

Supplementary Table S1 lists the platforms, sample numbers, and clinical endpoints for each HCC dataset. Data were analyzed using R software (version 4.0.3), R Bioconductor, and Python (version 3.8.8).

2.2 Genomic analysis of 26 m^{6}A regulators

The *oncoplot* function in the "maftools" R package [35] was used to analyze the mutational landscape of the genes encoding 26 m^{6}A regulatory factors in the TCGA-LIHC and ICGC-LIRI-JP cohorts. Results were depicted using the "ComplexHeatmap" R package [36]. The landscape of copy number variations in the 26 m^{6}A genes across human chromosomes was plotted using the "RCircos" R package [37].

2.3 Crosstalk among 26 m^{6}A methylation regulators

Protein-protein interactions (PPI) among the 26 m^{6}A regulators were analyzed using the STRING interaction database [38] and visualized using Cytoscape software (version 3.8.0) [39]. The size of each node reflects the number of regulatory factors that interact with it.

2.4 Unsupervised consensus clustering based on expression of m^{6}A methylation regulators

To identify distinct patterns of m^{6}A methylation, data on the expression of 26 m^{6}A regulator genes from previously published studies [40, 41] (Supplementary Table S2) were extracted from the four integrated HCC datasets mentioned above. Unsupervised clustering based on the expression data was used to categorize patients with the "ConsensuClusterPlus" R package [42]. Clustering was based on Euclidean distance and the k-means approach and was performed 1,000 times to ensure cluster stability.

2.5 Gene set variation analysis (GSVA) and gene set enrichment analysis (GSEA)

The activity of biological pathways in different patterns of m^{6}A modification was assessed using the "GSVA" R package [43]. Functions and pathways in patients expressing low or high levels of HNRNPA2B1 in the TCGA cohort were investigated using GSEA within the "fgsea" R package [44]. Gene sets showing a |normalized enrichment score| > 1 and $P < 0.05$ were considered significant enrichment for enrichment in Kyoto Encyclopedia of Genes and Genomes (KEGG) pathways and hallmark gene sets from the Molecular Signatures Database (version 7.5).

2.6 Single-sample GSEA (ssGSEA) to estimate abundance of immune cells in the TME

The relative abundances of 28 types of immune cells in the TME were quantified using ssGSEA within the "GSVA" R package based on well-defined gene signatures for each cell type [45] (Supplementary Table S3). Abundances were expressed on a normalized scale from 0 to 1.

2.7 Prediction of HCC response to immunotherapy

Likely response of HCC to immunotherapy was predicted using several published scoring systems. The immunophenoscore (IPS) score [45] was calculated by summing the weighted average of Z scores for the following four variables: (1) effector cells, defined as activated CD4$^+$ T lymphocytes, activated CD8$^+$ T lymphocytes, effector memory CD4$^+$ T lymphocytes, and effector memory CD8$^+$ T lymphocytes; (2) suppressive cells, defined as regulatory T cells (Tregs) and myeloid-derived suppressor cells (MDSCs); (3) MHC-associated molecules; and (4) use of immunomodulators or checkpoint inhibitors. Higher IPS suggests greater abundance of immune checkpoint molecules in the TME and therefore stronger immunogenicity and response to immunotherapy.

The "tumor immune dysfunction and exclusion" (TIDE) score was calculated as described [46]. Higher TIDE score suggests greater likelihood of immune escape by the tumor, implying weaker response to checkpoint inhibitors.

The algorithm "Estimation of stromal and immune cells in malignant tumors using expression data" (ESTIMATE) was applied to the data as described [47]. Scores were calculated for relative abundance of immune cells ("immune score"), stromal cells ("stromal score") and tumor cells ("tumor purity") in the TME. Lower tumor purity suggests greater abundance of stromal and immune cells than tumor cells, implying stronger response to immunotherapy.

2.8 Identification of differentially expressed genes (DEGs) between patterns of m^{6}A modification

Genes whose expression differed between patterns of m^{6}A modification were identified using the "limma" R package [31]. DEGs were defined as genes whose expression showed $|\log_2(\text{fold change})| > 0.5$ and $P < 0.05$ after Benjamini-Hochberg adjustment for multiple testing [48].

2.9 Enrichment of DEGs in defined functions and pathways

To explore the potential roles of the abovementioned DEGs, the DEGs were analyzed for enrichment in predefined functions and pathways using GSEA within the "clusterProfiler" R package [49]. The filtering criteria for GSEA are the same as in the previous description. GSEA results were visualized using the "enrichplot" R package.

2.10 Construction of gene signatures related to m^{6}A modification

Genes whose expression might predict overall survival of HCC patients were explored in the TCGA-LIHC cohort using Kaplan-Meier and univariate Cox regression. Prediction was considered significant if $P < 0.01$. Only genes satisfying this criterion were considered in subsequent analyses.

Next, we randomly divided the TCGA-LIHC cohort 1:1 into a training and test set using the *createDataPartition* function in the "caret" R package. Cox regression involving the least absolute shrinkage and selection operator (LASSO) was applied to the training set using the "glmnet" R package [50, 51]. The best penalty parameter lambda (λ) was determined through 10-fold cross validation, and the proportional hazard hypothesis was tested using the *cox.zph* function in the "survival" R package. Genes that did not meet the proportional hazard hypothesis were excluded from subsequent analyses.

Finally, multivariate Cox regression was performed on gene expression and patient survival data. A risk score was computed for each sample using the formula:

$$risk\ score = \sum_{i=1}^{n} \left(Coefficient_i * Expression_i\right),$$

where *Coefficient* refers to the regression coefficient and *Expression* to the gene's relative expression level. Based on the median risk score in the TCGA training set, patients from the TCGA training set, the TCGA testing set, the entire TCGA cohort as well as both GEO cohorts and the ICGC-LIRI-JP cohort were stratified into those at low or high risk. Patients in the IMvigor210 dataset were divided into high or low risk groups based on the optimal cutoff value of the risk score derived from the *surv_cutpoint* function in the "survminer" package in R.

2.11 Statistical analysis

All statistical analyses were performed using R version 4.0.3 (www.r-project.org). All *P* values were two-sided, with significance defined as $P < 0.05$ unless otherwise noted. Pairwise differences were assessed for significance using the nonparametric Wilcoxon rank-sum test, while differences among more than two groups were assessed using the nonparametric Kruskal-Wallis test. Associations between clinicopathological parameters and risk score were assessed using the chi-squared test.

Univariate Cox regression was used to assess hazard ratios (HRs) for 26 m^{6}A regulators, and correlations among the regulators were explored using the nonparametric Spearman test, with the results visualized in the "forestplot" R package. Survival curves were generated using the Kaplan-Meier approach, and curves were compared using the log-rank test. All heatmaps were generated using the R packages "pheatmap" (https://CRAN.R-project.org/package=pheatmap) and "ComplexHeatmap" [36].

3 Results

3.1 Multi-omics landscape of m^{6}A methylation regulators in HCC

The roles of 26 genes encoding proteins that regulate m^{6}A methylation in HCC were investigated in this study (Fig. 1A). The encoded proteins comprised nine "writers", which add the modification to RNA [METTL3, METTL14, METTL16 (or METT10D), WTAP, KIAA1429, ZC3H13, RBM15, RBM15B, and CBLL1]; three "erasers", which

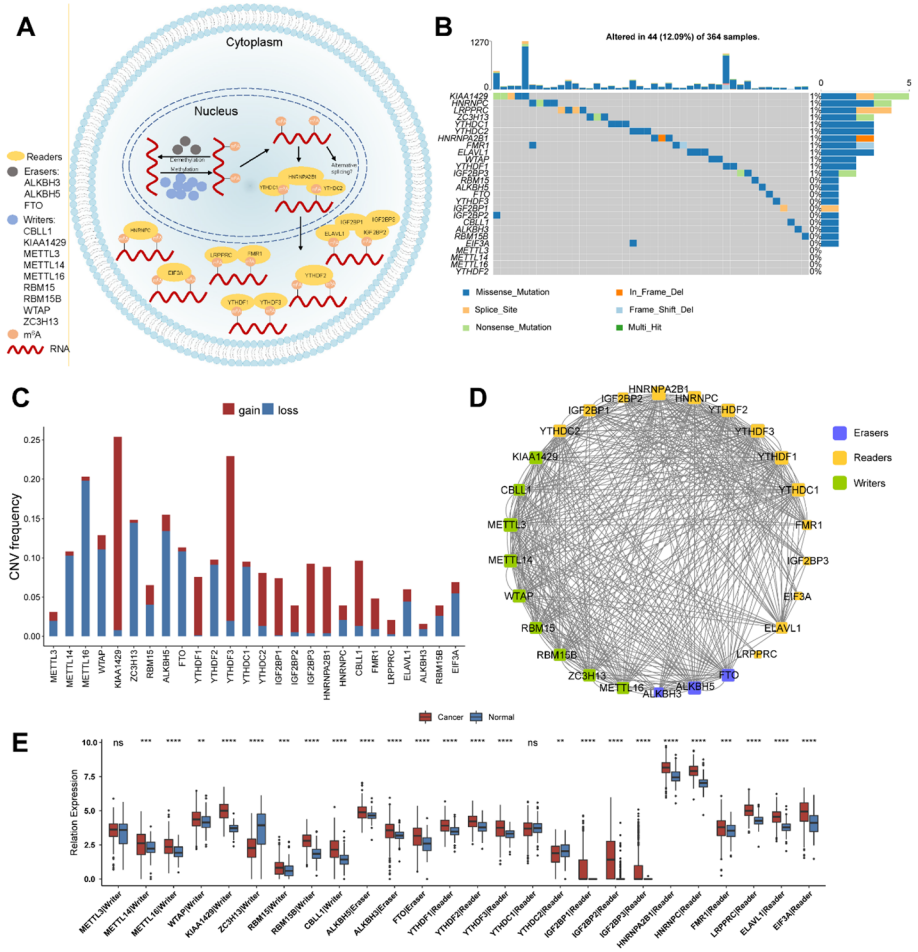

Fig. 1 Multi-omics landscape of m^{6}A regulators in HCC. **(A)** Overview of the 26 m^{6}A regulators and their biological processes in RNA metabolism. **(B)** The frequency of mutations in 26 m^{6}A modification regulators in the TCGA-LIHC cohort. Each column indicates an individual sample. The upper bar plot indicates tumor mutation burden (TMB). The number on the right shows the frequency of mutations for each regulator. The right bar displays the percentage of each type of genetic alteration. **(C)** The frequency of copy number variations (CNV) of 26 m^{6}A regulators in the TCGA-LIHC cohort. Amplification of the DNA copy number is shown in red and deletion of the copy number in blue. **(D)** The network of protein-protein interactions among 26 m^{6}A regulators. The size of each node reflects the number of proteins that interact with it. **(E)** Boxplot comparing the expression of 26 m^{6}A regulators between tumor and normal tissues. ns: not significant, *$P<0.05$, **$P<0.01$, ***$P<0.001$, ****$P<0.0001$

delete the modification (ALKBH3, ALKBH5, and FTO); and 14 "readers", which recognize the methylation (YTHDF1, YTHDF2, YTHDF3, YTHDC1, YTHDC2, IGF2BP1, IGF2BP2, IGF2BP3, HNRNPA2B1, HNRNPC, FMR1, LRPPRC, ELAVL1, and EIF3A). How these three groups of proteins dynamically modify RNA is unclear.

The total mutation rate of 26 m^6A regulators was relatively low in the HCC genomes of the TCGA cohort, where 44 samples had mutations (Fig. 1B), and the ICGC cohort, where 37 samples had mutations (Figure S2A). The most frequent alterations were missense mutations. In the TCGA cohort, KIAA1429 showed the greatest mutation frequency, followed by HNRNPC and LRPPRC (Fig. 1B). In the ICGC cohort, HNRNPA2B1 showed the highest mutation frequency, followed by KIAA1429 and EIF3A (Figure S2A).

Analysis of concurrent mutations across the 26 m^6A regulators revealed patterns of co-occurring mutations in YTHDC2 and EIF3A, IGF2BP2 and KIAA1429, as well as FMR1 and HNRNPC (Figure S2B). No evidence of mutually exclusive mutations was found among the 26 m^6A regulators (Figure S2B).

Analysis of copy number variation revealed that KIAA1429, YTHDF3, and HNRNPA2B1 had a relatively high frequency of amplification, while METTL16, METTL14, and ZC3H13 had frequent deletions (Fig. 1C). Figure S2C illustrates the chromosomal locations of copy number variations across the 26 m^6A regulators. Analysis based on the STRING database predicted extensive protein-protein interactions among the 26 m^6A regulators (Fig. 1D).

Most regulators were strongly elevated in HCC tissues, with the exception of ZC3H13 and YTHDC2 (Fig. 1E), implying that they play essential roles in the formation and progression of HCC. Most of the 26 m^6A regulators showed a strong positive co-expression relationship with one another in the TCGA cohort based on the Spearman correlation test (Figure S2D), in accord with the results in the four-cohort HCC dataset (Fig. 2A and Table S4).

Taken together, these findings suggest that genetic variation and abnormal expression of the 26 m^6A regulators may promote cell-cycle disturbance, genomic instability, and accumulation of genomic mutations during the development and progression of HCC.

3.2 Associations of m^6A regulators with patient prognosis and immune cell profiles in the TME

The prognostic value of 26 m^6A regulators was assessed for the four cohorts in our study using univariate Cox regression. Higher expression of most regulators, including RBM15B, YTHDF2 and LRPPRC, was associated with shorter overall survival, implying that they are risk factors of poor prognosis (Fig. 2A and S3A). Higher expression of ZC3H13, in contrast, was associated with longer overall survival, implying that it protects against poor prognosis. The positive co-expression among numerous m^6A regulators implies that crosstalk among the regulators may influence prognosis.

To better understand the role of these m^6A regulators in HCC, we explored interactions between their levels of expression and abundance of immune cell types in the TME. Expression of WTAP and ALKBH3 correlated positively with the relative abundance of most types of immune cells, whereas expression of the remaining m^6A regulators correlated negatively with abundance of most types of immune cells (Fig. 2B). Comparison of the expression of the 26 m^6A regulators in tumors of patients who showed complete

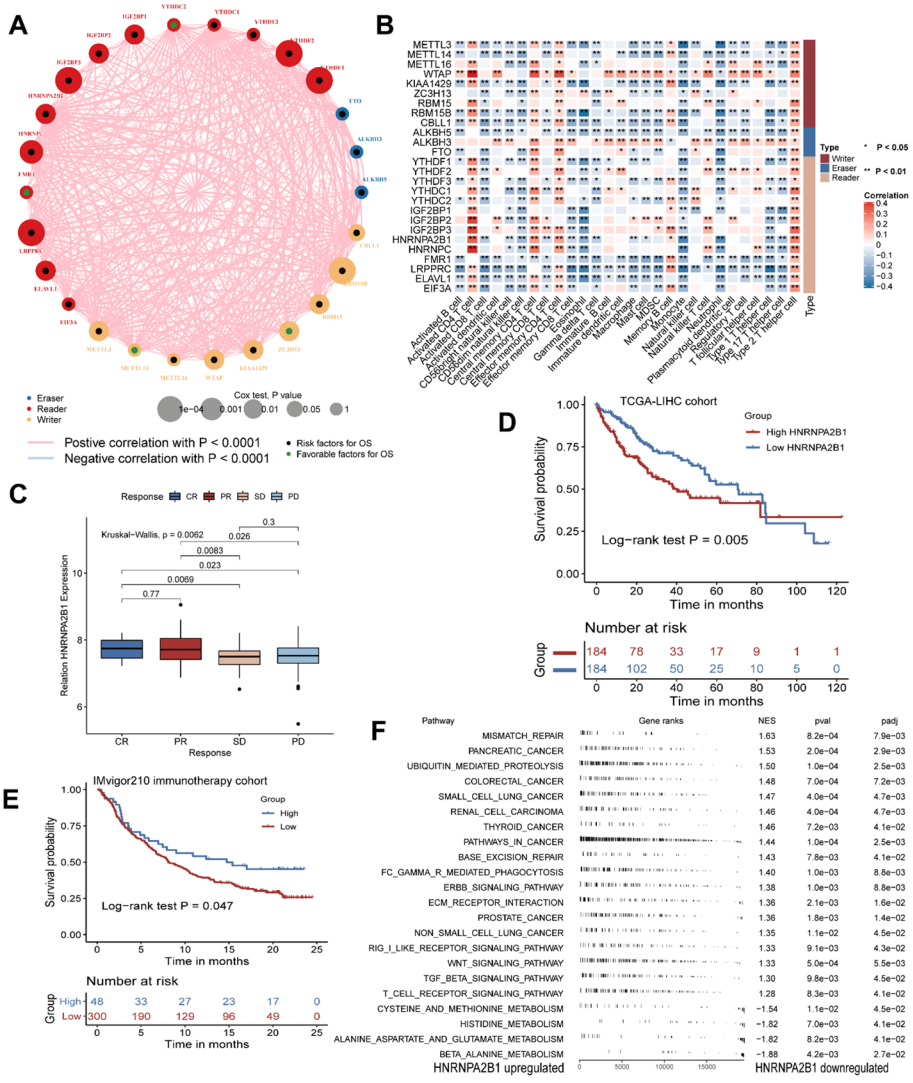

Fig. 2 Prognosis and immune characteristics of m^{6}A regulators. **(A)** Prognosis and correlation network diagram of 26 m^{6}A regulators in HCC patients. The red line indicates a positive correlation with $P < 0.0001$, whereas the blue line indicates a negative correlation with $P < 0.0001$. The size of the node reflects the P value of univariate Cox regression. Green points denote factors associated with higher overall survival; black points, factors associated with lower overall survival. **(B)** Heatmap of correlations between 26 m^{6}A regulators and 28 types of immune cells in the four-cohort HCC dataset. Red indicates a positive correlation, while blue indicates a negative correlation. $^*P < 0.05$, $^{**}P < 0.01$. **(C)** Boxplot of relative HNRNPA2B1 expression in tumors showing different responses to anti-PD-L1 immunotherapy. Kruskal-Wallis test, $P = 0.0062$. **(D)** Survival analysis of groups expressing high HNRNPA2B1 ($n = 184$) or low HNRNPA2B1 ($n = 184$) in the TCGA-LIHC cohort. Log-rank test, $P = 0.005$. **(E)** Survival analysis of groups expressing high HNRNPA2B1 ($n = 48$) or low HNRNPA2B1 ($n = 300$) in the IMvigor210 immunotherapy cohort. Log-rank test, $P = 0.047$. **(F)** In the TCGA-LIHC cohort, gene set enrichment analysis (GSEA) revealed that cancer- and immune-related pathways were enriched in the group expressing high HNRNPA2B1, while four metabolism-related pathways were enriched in the group expressing low HNRNPA2B1

or partial response or stable or progressive disease in the IMvigor210 cohort, which contained patients with various types of cancer on immunotherapy (Figure S4), revealed that expression of HNRNPA2B1 was higher in tumors showing complete or partial response (Fig. 2C). Patients in the TCGA-LIHC cohort with high HNRNPA2B1 expression showed shorter overall survival than those with low expression (Fig. 2D), yet those in the IMvigor210 cohort with high HNRNPA2B1 expression showed longer survival than those with low expression (Fig. 2E). GSEA analysis of the TCGA cohort linked high

HNRNPA2B1 expression to enrichment in several pathways related to cancer and immunity, such as the FC γ R-mediated phagocytosis and T cell receptor signaling (Fig. 2F).

These findings associate HNRNPA2B1 expression with HCC formation, progression and response to immunotherapy. The m^{6}A reader HNRNPA2B1 may be a biomarker for predicting immunotherapy response.

3.3 Patterns of m^{6}A methylation in HCC based on expression of the 26 m^{6}A regulators

HCC tissues in the four-cohort HCC dataset were stratified according to expression of 26 m^{6}A regulators using consensus clustering, and two patterns of m^{6}A methylation were found to provide the most effective clustering (Fig. 3A and B). Patients were therefore divided into two categories, Cluster 1 (C1, $n = 461$) and Cluster 2 (C2, $n = 318$). Most m^{6}A regulators showed relatively high expression in pattern C2 (Figure S3B and S3C), which was associated with significantly shorter overall survival than pattern C1 ($P < 0.0001$, log-rank test, Fig. 3C).

The two patterns C1 and C2 differed significantly in the relative abundance of various types of immune cells in the TME (Table S5). Even though C2 was associated with worse survival (Fig. 3D), it was associated with significantly greater abundance of activated CD4$^+$ T cells, effector memory CD4$^+$ T cells and natural killer T cells, as well as with significantly lower abundance of regulatory T cells, type 1 helper T cells and monocytes. Pattern C1, for its part, was associated with relatively high proportions of activated CD8$^+$ T cells and effector memory CD8$^+$ T cells.

The ESTIMATE algorithm showed that pattern C1 was associated with higher stromal scores than pattern C2 (Fig. 4A, $P = 0.00021$), while C2 showed greater tumor purity

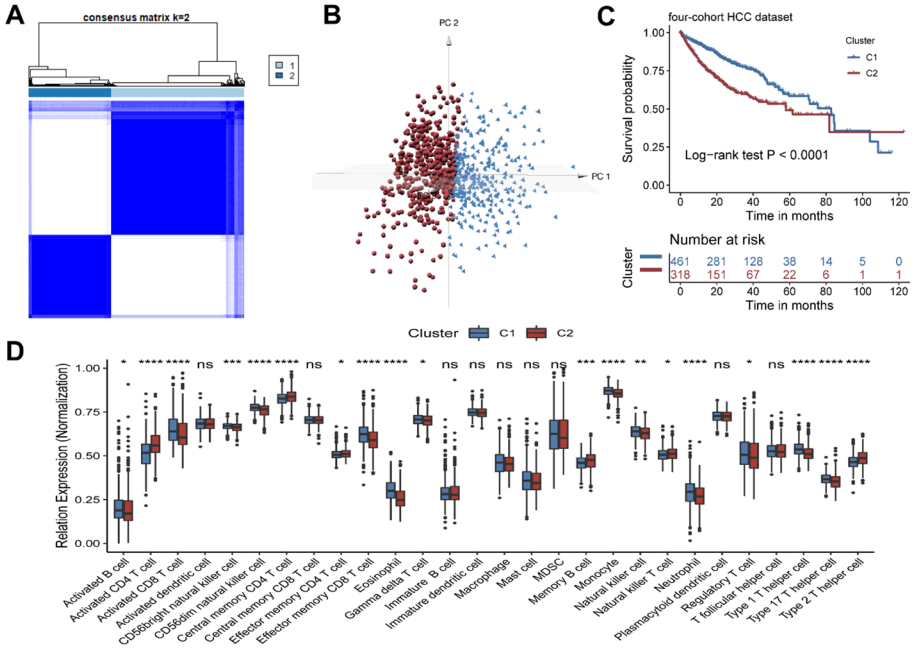

Fig. 3 m^{6}A methylation modification patterns in the four-cohort HCC dataset. **(A)** Consensus clustering matrix of 779 patients with k = 2. **(B)** Three-dimensional principal component analysis (3D-PCA) of 26 m^{6}A regulators to identify two m^{6}A methylation patterns in 779 patients from four cohorts. **(C)** Kaplan-Meier curves of the two m^{6}A modification patterns involving 461 cases of m^{6}A modification pattern C1, and 318 cases of m^{6}A modification pattern C2. Log-rank test, $P < 0.0001$. **(D)** Boxplot depicting relative immune cell abundance in the two m^{6}A modification patterns. ns: not significant, *$P < 0.05$, **$P < 0.01$, ***$P < 0.001$, ****$P < 0.0001$

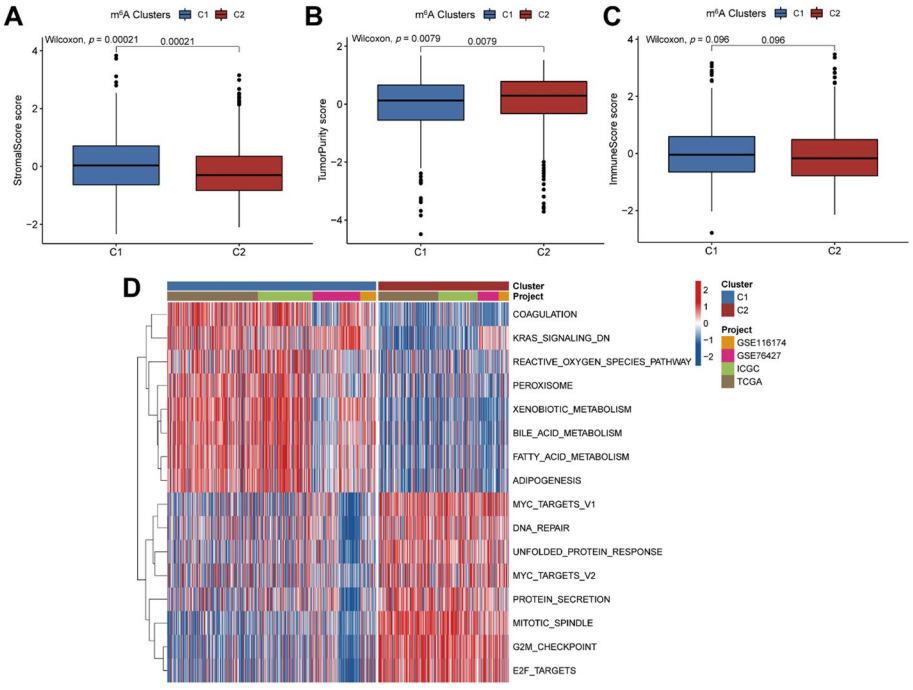

Fig. 4 Tumor microenvironment characteristics in different m^{6}A modification patterns. **(A)** Boxplot of tumor purity in the two distinct m^{6}A modification patterns in the four-cohort HCC dataset. Wilcoxon rank sum test, $P = 0.0079$. **(B)** The stromal score of two m^{6}A modification patterns were analyzed and plotted. Wilcoxon rank sum test, $P = 0.00021$. **(C)** Comparison of immune score of two m^{6}A modification patterns. Wilcoxon rank sum test, $P = 0.096$. **(D)** Gene set variation analysis (GSVA) of relative activation of hallmark gene sets in two m^{6}A modification patterns. Red indicates activated pathways, and blue indicates inhibited pathways

(Fig. 4B, $P = 0.0079$). Immune score did not differ significantly between the two patterns (Fig. 4C, $P = 0.096$).

Pattern C1 was significantly enriched in metabolic pathways, such as those involving metabolism of xenobiotics, bile acids and fatty acids (Fig. 4D and Table S6). C2, in contrast, was markedly enhanced in pathways related to the cell cycle, such as those involving the MYC targets V1/V2, DNA repair, and E2F targets. These results link pattern C2 to cancer activation status.

3.4 Associations of the two m^{6}A methylation patterns with clinical and transcriptomic characteristics in the TCGA-LIHC cohort

Consensus clustering of patients in the TCGA-LIHC cohort according to expression of the 26 m^{6}A regulators revealed two m^{6}A modification patterns similar to those identified above in the combination of four cohorts (Fig. 5A and S5A, S5B and S5C). Pattern C2 was associated with higher expression of all m^{6}A regulators except the eraser ALKBH3 (Figure S5C). Pattern C1 was associated with better overall survival than C2 (log-rank test, $P = 0.003$; Fig. 5B).

In the TCGA-LIHC cohort, comparison of the immune cell landscape in the TME between the two m^{6}A methylation profiles using ssGSEA revealed similar differences in relative abundance of activated CD4$^+$ T cells, activated CD8$^+$ T cells, effector memory CD8$^+$ T cells, and type 2 helper T cells as in the above analysis involving all four cohorts (Figure S5D). Based on several immune infiltration-related signatures from previous work [52] (Table S7), pattern C1 appeared to be enriched in immune responses involving

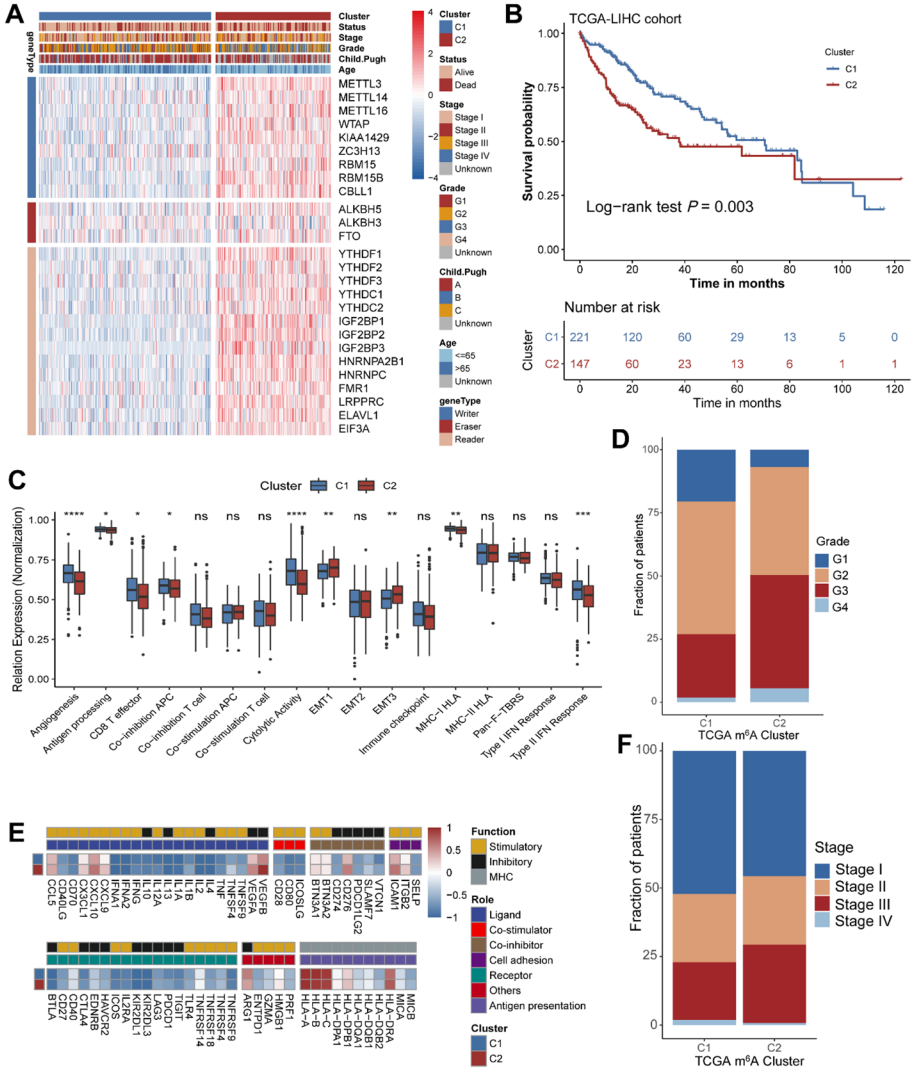

Fig. 5 Different clinical and transcriptional characteristics associated with the two m^{6}A modification patterns in the TCGA-LIHC cohort. **(A)** Heatmap shows the expression of 26 m^{6}A regulators. Red denotes high expression, and blue denotes low expression. Samples were annotated by m^{6}A modification pattern, overall status, stage, histology grade, Child-Pugh grade, and age. **(B)** Kaplan-Meier curves of two m^{6}A modification patterns involving 221 cases of m^{6}A modification pattern C1 and 147 cases of pattern C2. Log-rank test, $P = 0.003$. **(C)** Fractions of 17 immune signatures in the two m^{6}A modification patterns. ns: not significant, $^*P < 0.05$, $^{**}P < 0.01$, $^{***}P < 0.001$, $^{****}P < 0.0001$. **(D)** Stacked bar plot of histology grade in the two m^{6}A modification patterns. G1, blue; G2, orange; G3, red; G4, light blue. **(E)** Heatmap depicting the average differences in immune-related gene expression between the two m^{6}A modification patterns. Red squares represent upregulation, while blue squares represent downregulation. **(F)** Proportions of different "tumor, lymph node, metastasis" (TNM) stages in the two m^{6}A modification patterns. Stage I, blue; stage II, orange; stage III, red; stage IV, light blue

CD8$^+$ T effector cells, angiogenesis, cytolytic activity, and type II interferon (Fig. 5C). Pattern C2, in contrast, featured higher expression of epithelial-mesenchymal transition (EMT) 1 and EMT 3. Further comparison of the expression of immune-related genes between patterns C1 and C2 (Fig. 5E) revealed relatively high expression of several ligands (such as CXCL10, CXCL9, VEGFA, and VEGFB), co-inhibitor CD276, and cell adhesion molecules (ITGB2 and ICAM1) in pattern C2.

In the TCGA-LIHC cohort, many patients with advanced HCC showed pattern C2, whereas most patients with lower histology grades showed pattern C1 (Fig. 5D and F),

implying that C2 may be associated with HCC progression. Indeed, pattern C2 was associated with significantly higher stemness mRNAsi (Figure S6A).

These findings suggested that HCC patients could be classified into two molecular subtypes based on the expression of 26 m^6A regulators. In the two subtypes, pattern C1 indicated a high proportion of infiltrating $CD8^+$ T cell and stromal cells in the TME, and it was associated with favorable prognosis. Pattern C2 indicated high proportions of infiltrating $CD4^+$ T cells and type 2 helper T cells as well as high tumor purity, and it was associated with malignant progression and poor prognosis.

3.5 DEGs between m^6A methylation patterns in HCC and their selection for a potential prognostic gene signature

To explore how the two patterns of m^6A methylation in HCC may translate to different tumor phenotypes, an empirical Bayesian approach was used to identify 2887 DEGs between the two patterns (Figure S6B). GSEA between patterns C1 and C2 linked C2 to enrichment in pathways related to the cell cycle, such as pathways involving E2F targets, the G2M checkpoint, the MYC target V1, TGF-β and the EMT, which was consistent with previous analyses (Fig. 6A).

Of the 2887 DEGs, 861 showed prognostic value based on Kaplan-Meier analysis and univariate Cox regression (Table S8). Unsupervised clustering analysis based on the expression of these 861 genes assigned HCC patients to one of two patterns, which we termed "m^6A methylation-related gene patterns" (Fig. 6B and S6C). Gene pattern B was associated with worse prognosis and higher histology grade than gene pattern A (Fig. 6B C). Expression of immune-related genes in gene patterns A and B were remarkably similar to that in the two m^6A methylation patterns C1 and C2 in the TCGA-LIHC cohort (Fig. 6D). Gene pattern A was associated with greater expression of angiogenesis and type I/II interferon response signatures, whereas gene pattern B was associated with greater expression of EMT1/3, immune checkpoint, and MHC-II HLA signatures (Figure S6D). These results further support that the two m^6A methylation patterns correspond to two molecular subtypes of HCC differing in clinical characteristics and infiltration of the TME by immune cells.

In order to define an "m^6A signature" that might predict prognosis, LASSO Cox regression was performed on the 861 DEGs related to prognosis, and the regression coefficient of each gene was estimated using an optimal lambda (λ) derived from 10-fold cross validation (Figure S7A and S7B). Based on the resulting m^6A signature, patients were assigned to low- or high-risk groups using a median cutoff value of 0.8434 in the case of the TCGA training set or an optimal threshold value of 4.1580 in the case of the IMvigor210 cohort.

3.6 Ability of the m^6A signature to predict clinical features and prognosis

Patients who were assigned to the low-risk group based on the m^6A signature showed favorable overall survival, whether in the TCGA-LIHC training set ($P<0.001$), TCGA-LIHC test set ($P<0.001$), entire TCGA-LIHC cohort ($P<0.001$; Fig. 7A and C), ICGC cohort ($P<0.001$; Fig. 7D), the combination of all four cohorts ($P<0.001$; Fig. 7E), the GSE116174 cohort ($P=0.002$; Fig. 7F), or the IMvigor210 cohort ($P=0.019$, Fig. 7G). However, the survival advantage of being in the low-risk group did not achieve statistical significance in the GSE76472 cohort ($P=0.541$; Fig. 7H).

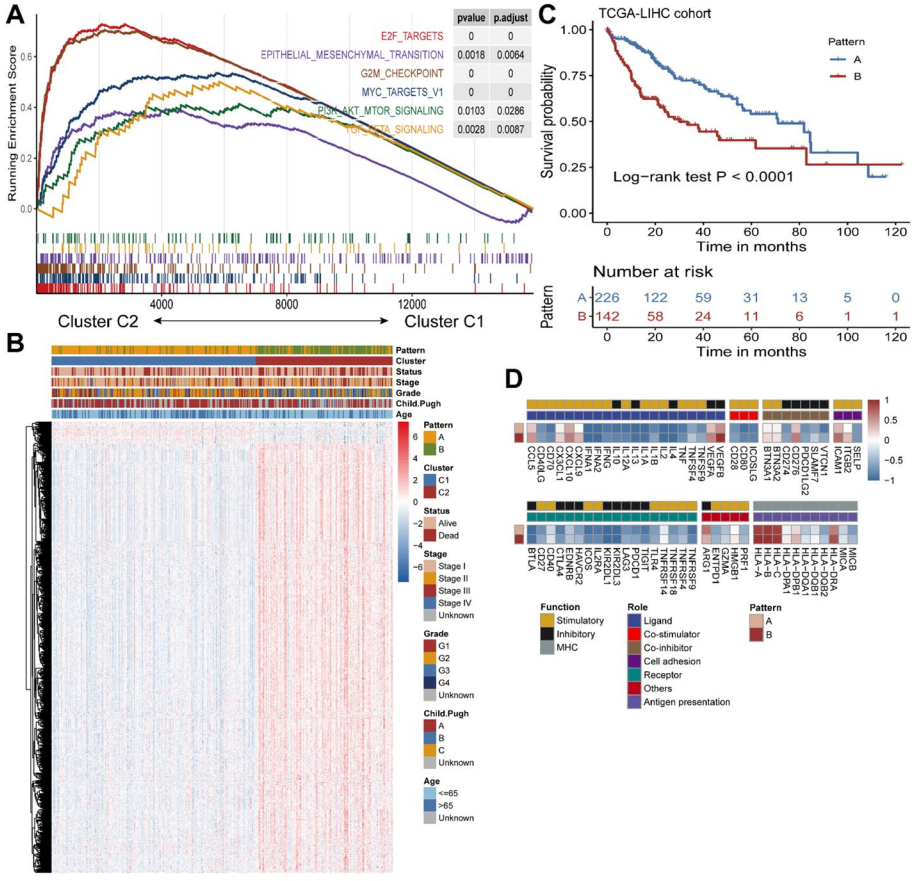

Fig. 6 Transcriptomic characteristics and functional annotation of genes differentially expressed between the two m^{6}A modification patterns. **(A)** Gene set enrichment analysis (GSEA) plots showing enrichment of the following gene sets in m^{6}A modification-related gene pattern B: E2F targets (red), epithelial-mesenchymal transition (purple), G2M checkpoint (brown), MYC target V1 (cyan), PI3K-AKT-mtor signaling (green), and TGF-β signaling (orange). **(B)** Unsupervised clustering of 861 genes associated with m^{6}A modification in the TCGA-LIHC cohort. Annotations along the top refer to m^{6}A modification pattern, overall survival status, stage, histology grade, Child-Pugh grade, and age. Red denotes high expression, and blue denotes low expression. **(C)** Kaplan-Meier curves of two m^{6}A modification-related gene patterns involving 226 cases in gene pattern A, and 142 cases in gene pattern B. Log-rank test, $P < 0.0001$. **(D)** Heatmap showing the average differences in expression of immune-related genes in two m^{6}A modification-related gene patterns. Red squares represent upregulation, while blue squares represent downregulation

Tumor mutation burden (TMB) may be useful for predicting response to checkpoint immunotherapy [53], so we compared TMB between high- and low-risk groups in the TCGA-LIHC cohort. TMB was significantly higher in the high-risk group ($P = 0.0016$; Fig. 7I), which had a relatively high level of neo-antigens. At the same time, risk score correlated positively with mRNAsi ($R = 0.49$, $P < 0.001$; Figure S7C), which may help explain the poor prognosis in the high-risk group.

The score on the m^{6}A signature also correlated with at least some clinical characteristics of HCC patients. The low-risk group showed earlier staging and histology grade in the TCGA cohort (Fig. 8A, $^{***}P < 0.001$) and the ICGC cohort (Fig. 8B, $^{***}P < 0.001$). Risk type based on the m^{6}A signature correlated with m^{6}A methylation pattern, m^{6}A methylation-related gene pattern, and overall survival (Fig. 8C and Table S9). Multivariate Cox regression confirmed the m^{6}A signature to be an independent predictor of overall survival in the TCGA and ICGC cohorts (Fig. 9A and B).

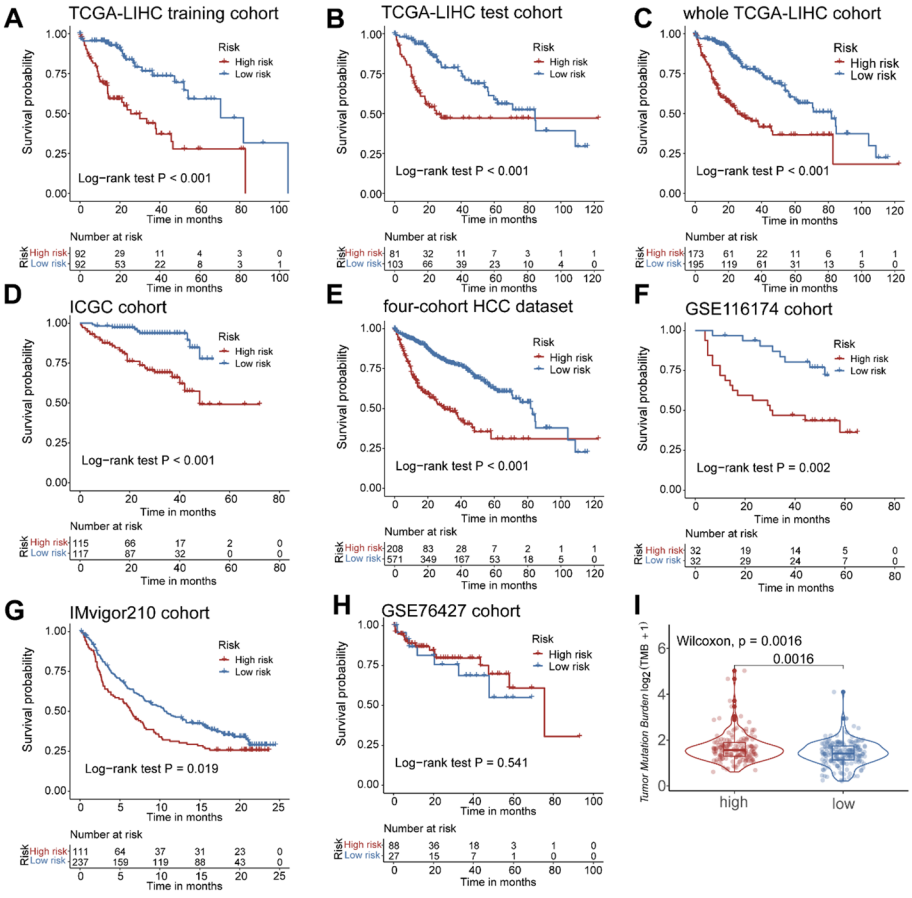

Fig. 7 Prognostic value of the risk score in multiple HCC cohorts. **(A)** Kaplan-Meier survival analysis of patients in the TCGA training cohort stratified into groups at high risk ($n=92$) or low risk ($n=92$). Log-rank test, $P<0.001$. **(B)** Kaplan-Meier survival analysis of patients in the TCGA test cohort stratified into high risk ($n=81$) or low risk ($n=103$). Log-rank test, $P<0.001$. **(C)** Kaplan-Meier survival analysis of patients in the whole TCGA cohort stratified into groups at high risk ($n=173$) or low risk ($n=195$). Log-rank test, $P<0.001$. **(D)** Kaplan-Meier survival analysis of patients in the ICGC cohort stratified into groups at high risk ($n=115$) or low risk ($n=117$). Log-rank test, $P<0.001$. **(E)** Kaplan-Meier survival analysis of patients in the four-cohort HCC dataset stratified into groups at high risk ($n=208$) or low risk ($n=571$). Log-rank test, $P<0.001$. **(F)** Kaplan-Meier survival analysis of patients in the GSE116174 cohort stratified into groups at high risk ($n=32$) or low risk ($n=32$). Log-rank test, $P=0.002$. **(G)** Kaplan-Meier survival analysis of patients in the IMvigor210 immunotherapy cohort stratified into groups at high risk ($n=111$) or low risk ($n=237$). Log-rank test, $P=0.019$. **(H)** Kaplan-Meier survival analysis of patients in the GSE76427 cohort stratified into groups at high risk ($n=88$) or low risk ($n=27$). Log-rank test, $P=0.541$. **(I)** Box violin plot of tumor mutation burden (TMB) in the TCGA-LIHC cohort stratified into groups at high risk or low risk. Wilcoxon rank sum test, $P=0.0016$

These results indicate that the m^{6}A signature may be useful for predicting at least some of the clinical features of HCC and overall survival of patients.

3.7 Ability of the m^{6}A signature to predict response to immunotherapy

While prediction of tumor response to immunotherapy has so far relied mainly on PD-L1 expression, TMB, and microsatellite instability [18, 54], other indices such as TIDE and IPS may be useful. In both the combination of all four cohorts and the TCGA-LIHC cohort on its own, low risk on the m^{6}A signature was associated with significantly lower TIDE (both $P<0.001$, Fig. 9C and D) and significantly higher IPS (both $P<0.001$, Fig. 9E and F). These results suggest that m^{6}A methylation may help regulate HCC response to immunotherapy.

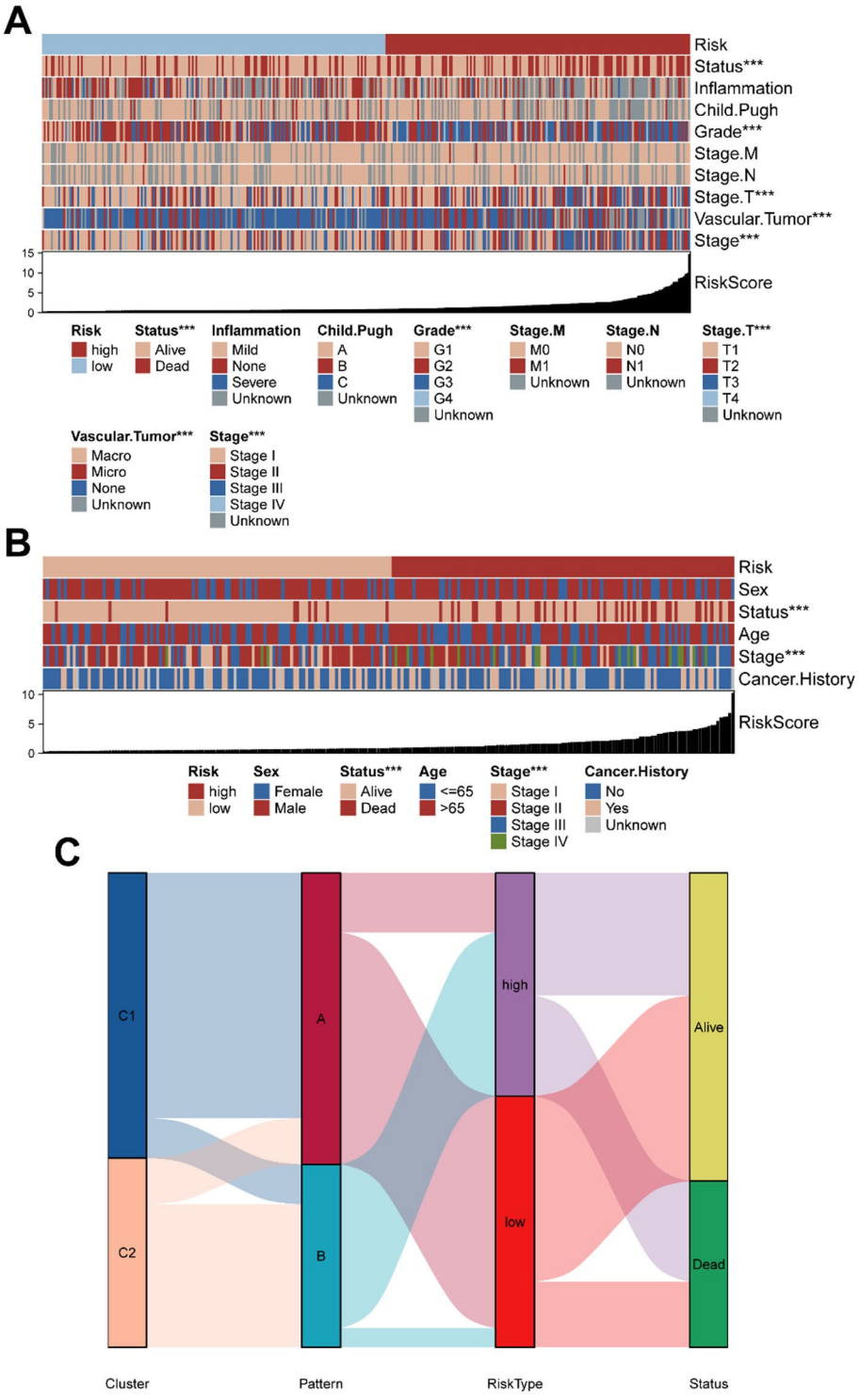

Fig. 8 Correlations between clinical characteristics and risk score in HCC. **(A)** Bar chart showing the relationship between risk scores and various clinical features in the TCGA-LIHC cohort. Samples are annotated with risk type, overall status, inflammation, Child-Pugh grade, histology grade, stage M, stage N, stage T, tumor vascularization, and stage. **(B)** Bar chart showing the relationship between risk scores and various clinical characteristics in the ICGC-LIRI-JP cohort. Samples are annotated with risk type, sex, overall survival status, age, stage, and cancer history. **(C)** Sankey diagram illustrating relationships among m^6A modification patterns, m^6A modification-related gene patterns, risk group, and overall survival status. Metastasis, M; Lymph node, N; Tumor, T

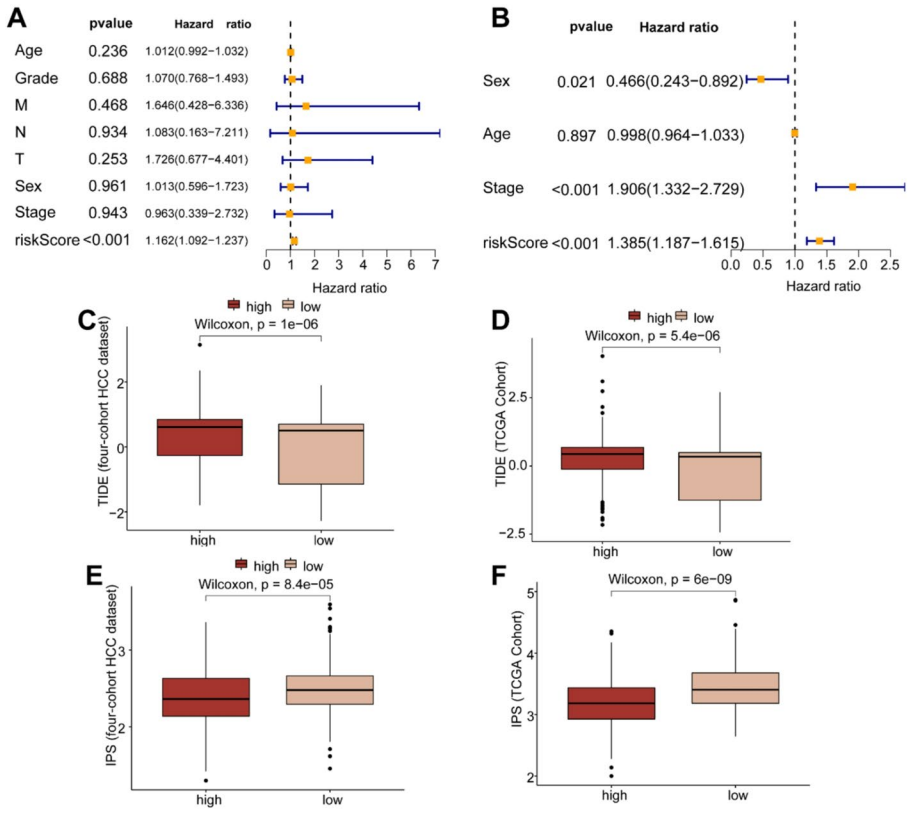

Fig. 9 The risk score is a biomarker of response to immunotherapy and prognosis. **(A)** Forest plot of multivariate Cox regression of risk score in the TCGA-LIHC cohort. The horizontal line denotes the 95% confidence interval for each group. The vertical dotted line represents a hazard ratio (HR) = 1. **(B)** Forest plot of multivariate Cox regression of risk score in the ICGC-LIRI-JP cohort. The horizontal line denotes the 95% confidence interval for each group. The vertical dotted line represents HR = 1. **(C)** Boxplot of "tumor immune dysfunction and exclusion" (TIDE) score for different risk score groups in the four-cohort HCC dataset. Wilcoxon rank sum test, $P < 0.001$. **(D)** Boxplot of TIDE scores for different risk score groups in the TCGA-LIHC cohort. Wilcoxon rank sum test, $P < 0.001$. **(E)** Comparison of the relative distribution of immunophenoscore (IPS) between high- and low-risk groups in the four-cohort HCC dataset. Wilcoxon rank sum test, $P < 0.001$. **(F)** Comparison of the relative distribution of IPS between high- and low-risk groups in the TCGA-LIHC cohort. Wilcoxon rank sum test, $P < 0.001$

4 Discussion

Growing evidence suggests that m^{6}A methylation plays a vital role in host responses to tumors such as HCC [22, 55] as well as in tumor responses to immune checkpoint blockade therapy. Therefore, identifying distinct patterns of m^{6}A modification in HCC may help clarify infiltration of the TME by immune cells and the personalization of therapeutic regimens. Here we identified two patterns of m^{6}A modification based on expression of 26 m^{6}A regulators, which were associated with different interactions between tumor cells and immune cells as well as with different clinical characteristics and overall survival.

Overall mutation rates of 26 m^{6}A regulators were found to be relatively low in the HCC genome. The m^{6}A modification pattern C1 was associated with better survival, and it was characterized by activation of metabolic pathways and a higher proportion of activated CD8$^+$ T cells, effector memory CD8$^+$ T cells, and stroma cell infiltration. Pattern C2, in contrast, was characterized by TGF-β signaling, the G2M checkpoint, E2F targets, and greater TME infiltration by CD4$^+$ T effector cells and type 2 helper T cells. In pattern C2, most of the m^{6}A regulators showed higher expression, implying that

upregulation of m^6A regulators may contribute to the progression of HCC. Although m^6A methylation regulator pattern C2 also showed high infiltration by activated $CD4^+$ T cells and other immune cell types, the activation of several cancer-related pathways and a greater infiltration by type 2 helper T cells might promote the progression of HCC and inhibit the activation of anti-tumor lymphocyte cells, leading to poor prognosis. Moreover, pattern C2 was associated with higher mRNAsi and tumor purity than C1, implying cancer activation status in C2. Pattern C2 was also enriched in EMT and TGF-β pathways of stroma activation.

Considering the different expression of HNRNPA2B1 among cancer patients showing four different responses to immunotherapy, we explored the biological significance behind the reader HNRNPA2B1. HNRNPA2B1 is an RNA-binding protein that is involved in microRNA processing and alternative splicing of transcripts in the nucleus [56]. The high expression of HNRNPA2B1 correlated with several cancer-related pathways and poorer prognosis. These results indicate that HNRNPA2B1 may be involved in the progression of HCC and serve as a potential biomarker for the response to immune checkpoint blockade therapy.

DEGs between the two m^6A methylation patterns were identified and were considered as m^6A phenotype-related genes. Two m^6A methylation gene patterns were identified based on these m^6A phenotype-related genes and were found to be significantly associated with different profiles of immune cells in the TME and different overall survival. These findings support the existence of two molecular subgroups of HCC similar to the m^6A methylation regulator patterns.

Based on the different m^6A methylation regulator patterns, we defined an m^6A signature to quantify risk of poor prognosis, which we validated in multiple HCC cohorts as well as a pan-cancer immunotherapy cohort. The risk score correlated strongly with IPS and TIDE, predictors of immune checkpoint blockade therapy. These findings imply that m^6A modification can influence the efficacy of immunotherapy. The m^6A signature may also be useful for assessing TMB, clinical stage, histology grade and other clinicopathological characteristics of HCC patients.

However, our research has several limitations that cannot be ignored. First, our findings are based on bioinformatic analyses of publicly available data, and clinical validation is required. Second, to enhance the reliability of the m^6A modification patterns, a series of newly identified m^6A regulators should be incorporated into an unsupervised clustering algorithm in future studies. Third, due to the absence of suitable immunotherapy cohorts based on the HCC cancer dataset, the risk prognostic model was only validated in a pan-cancer immunotherapy cohort. Thus, future assessment of its performance in predicting the efficacy of immune checkpoint blockade therapy across multiple HCC immunotherapy cohorts is indeed necessary. Fourth, HCC patients were stratified using the median cutoff of the risk score in the TCGA training set, and it is essential to confirm the optimized cutoff value of the risk score to better stratify HCC patients. Additionally, molecular experiments are needed to validate the specific biological pathways linking the expression of HNRNPA2B1 to the response to PD1/L1 or CTLA-4-targeted checkpoint immunotherapy.

5 Conclusions

We comprehensively evaluated the expression of 26 m^6A regulators in 779 HCC samples and defined two molecular subtypes of the cancer. We systematically explored the relationship between these two m^6A methylation patterns and characteristics of TME infiltration by immune cells. The results may provide insights into how m^6A methylation relates to TME characteristics and promote the development of new therapies against HCC.

Abbreviations

CNV	copy number variation
DEGs	differentially expressed genes
GSEA	gene set enrichment analysis
GSVA	gene set variation analysis
HCC	hepatocellular carcinoma
HR	hazard ratio
IPS	immunophenoscore
LASSO	least absolute shrinkage and selection operator
LIHC	liver hepatocellular carcinoma
PCA	principal component analysis
PPI	protein-protein interaction
ssGSEA	single-sample gene set enrichment analysis
TIDE	tumor immune dysfunction and exclusion
TMB	tumor mutation burden
TME	tumor microenvironment

Supplementary Information

The online version contains supplementary material available at https://doi.org/10.1007/s12672-025-02965-7.

Supplementary Material 1

Supplementary Material 2

Acknowledgements

We would like to thank the patients, investigators, clinicians, technical personnel, and funding bodies who contributed to the TCGA, GEO, ICGC, and UCSC Xena databases and made the information public. Without these data, the present study would not have been possible.

Author contributions

Z.Y. made substantial contributions to this study. Z.Y. conceived, designed, integrated, analyzed, visualized, and interpreted the data. Z.Y. wrote the manuscript, which Z.Y., L.H., M.H., L.W., and Y.Z. revised. Y.Z. supervised this study and provided financial support. All authors contributed to the article and approved the final manuscript.

Funding

This research did not receive any specific grant from funding agencies in the public, commercial, or not-for-profit sectors.

Data availability

The following publicly available datasets were analyzed in this study: TCGA, https://portal.gdc.cancer.gov; GEO, www.ncbi.nlm.nih.gov/geo; ICGC, https://icgc.org; and UCSC Xena, https://xena.ucsc.edu.

Declarations

Ethics approval and consent to participate

Not applicable.

Competing interests

The authors declare no competing interests.

Received: 9 February 2025 / Accepted: 10 June 2025

Published online: 14 June 2025

References

1. Roundtree IA, Evans ME, Pan T, He C. Dynamic RNA modifications in gene expression regulation. Cell. 2017;169:1187–200.
2. Fang F, Wang X, Li Z, Ni K, Xiong C. Epigenetic regulation of mRNA N6-methyladenosine modifications in mammalian gametogenesis. Mol Hum Reprod. 2021; 27:gaab025.

3. Niu Y, Zhao X, Wu YS, Li MM, Wang XJ, Yang YG. N6-methyl-adenosine (m6A) in RNA: an old modification with a novel epigenetic function. Genomics Proteom Bioinf. 2013;11:8–17.
4. Chen XY, Zhang J, Zhu JS. The role of m(6)A RNA methylation in human cancer. Mol Cancer. 2019;18:103.
5. He L, Li H, Wu A, Peng Y, Shu G, Yin G. Functions of N6-methyladenosine and its role in cancer. Mol Cancer. 2019;18:176.
6. Shi H, Wei J, He C. Where, when, and how: Context-Dependent functions of RNA methylation writers, readers, and erasers. Mol Cell. 2019;74:640–50.
7. Frye M, Harada BT, Behm M, He C. RNA modifications modulate gene expression during development. Science. 2018;361:1346–9.
8. Müller S, Glaß M, Singh AK, Haase J, Bley N, Fuchs T, et al. IGF2BP1 promotes SRF-dependent transcription in cancer in a m6A- and miRNA-dependent manner. Nucleic Acids Res. 2019;47:375–90.
9. Wang T, Kong S, Tao M, Ju S. The potential role of RNA N6-methyladenosine in Cancer progression. Mol Cancer. 2020;19:88.
10. Kwok CT, Marshall AD, Rasko JE, Wong JJ. Genetic alterations of m(6)A regulators predict poorer survival in acute myeloid leukemia. J Hematol Oncol. 2017;10:39.
11. Li M, Zha X, Wang S. The role of N6-methyladenosine mRNA in the tumor microenvironment. Biochim Biophys Acta Rev Cancer. 2021;1875:188522.
12. Bray F, Ferlay J, Soerjomataram I, Siegel RL, Torre LA, Jemal A. Global cancer statistics 2018: GLOBOCAN estimates of incidence and mortality worldwide for 36 cancers in 185 countries. CA Cancer J Clin. 2018;68:394–424.
13. Yuen MF, Chen DS, Dusheiko GM, Janssen HLA, Lau DTY, Locarnini SA, et al. Hepatitis B virus infection. Nat Rev Dis Primers. 2018;4:18035.
14. Péneau C, Imbeaud S, La Bella T, Hirsch TZ, Caruso S, Calderaro J, et al. Hepatitis B virus integrations promote local and distant oncogenic driver alterations in hepatocellular carcinoma. Gut. 2022;71:616–26.
15. Lei X, Lei Y, Li JK, Du WX, Li RG, Yang J, et al. Immune cells within the tumor microenvironment: biological functions and roles in cancer immunotherapy. Cancer Lett. 2020;470:126–33.
16. Hanahan D, Coussens LM. Accessories to the crime: functions of cells recruited to the tumor microenvironment. Cancer Cell. 2012;21:309–22.
17. Petitprez F, Vano YA, Becht E, Giraldo NA, de Reyniès A, Sautès-Fridman C, et al. Transcriptomic analysis of the tumor microenvironment to guide prognosis and immunotherapies. Cancer Immunol Immunother. 2018;67:981–8.
18. Pinter M, Jain RK, Duda DG. The current landscape of immune checkpoint Blockade in hepatocellular carcinoma: A review. JAMA Oncol. 2021;7:113–23.
19. Hugo W, Zaretsky JM, Sun L, Song C, Moreno BH, Hu-Lieskovan S, et al. Genomic and transcriptomic features of response to Anti-PD-1 therapy in metastatic melanoma. Cell. 2016;165:35–44.
20. Rizvi NA, Hellmann MD, Snyder A, Kvistborg P, Makarov V, Havel JJ, et al. Cancer immunology. Mutational landscape determines sensitivity to PD-1 Blockade in non-small cell lung cancer. Science. 2015;348:124–8.
21. Ferris RL, Blumenschein G Jr., Fayette J, Guigay J, Colevas AD, Licitra L, et al. Nivolumab for recurrent Squamous-Cell carcinoma of the head and neck. N Engl J Med. 2016;375:1856–67.
22. Gu Y, Wu X, Zhang J, Fang Y, Pan Y, Shu Y, et al. The evolving landscape of N(6)-methyladenosine modification in the tumor microenvironment. Mol Ther. 2021;29:1703–15.
23. Petitprez F, Meylan M, de Reyniès A, Sautès-Fridman C, Fridman WH. The tumor microenvironment in the response to immune checkpoint Blockade therapies. Front Immunol. 2020;11:784.
24. Grinchuk OV, Yenamandra SP, Iyer R, Singh M, Lee HK, Lim KH, et al. Tumor-adjacent tissue co-expression profile analysis reveals pro-oncogenic ribosomal gene signature for prognosis of resectable hepatocellular carcinoma. Mol Oncol. 2018;12:89–113.
25. Shiraishi Y, Fujimoto A, Furuta M, Tanaka H, Chiba K, Boroevich KA, et al. Integrated analysis of whole genome and transcriptome sequencing reveals diverse transcriptomic aberrations driven by somatic genomic changes in liver cancers. PLoS ONE. 2014;9:e114263.
26. Fujimoto A, Furuta M, Totoki Y, Tsunoda T, Kato M, Shiraishi Y, et al. Whole-genome mutational landscape and characterization of noncoding and structural mutations in liver cancer. Nat Genet. 2016;48:500–9.
27. Du P, Kibbe WA, Lin SM. Lumi: a pipeline for processing illumina microarray. Bioinformatics. 2008;24:1547–8.
28. Gautier L, Cope L, Bolstad BM, Irizarry RA. affy–analysis of affymetrix genechip data at the probe level. Bioinformatics. 2004;20:307–15.
29. Wagner GP, Kin K, Lynch VJ. Measurement of mRNA abundance using RNA-seq data: RPKM measure is inconsistent among samples. Theory Biosci. 2012;131:281–5.
30. Koboldt DC, Larson DE, Wilson RK. Using VarScan 2 for germline variant calling and somatic mutation detection. Curr Protoc Bioinf. 2013; 44:15.4.1-7.
31. Ritchie ME, Phipson B, Wu D, Hu Y, Law CW, Shi W, et al. Limma powers differential expression analyses for RNA-sequencing and microarray studies. Nucleic Acids Res. 2015;43:e47.
32. Vivian J, Rao AA, Nothaft FA, Ketchum C, Armstrong J, Novak A, et al. Toil enables reproducible, open source, big biomedical data analyses. Nat Biotechnol. 2017;35:314–6.
33. Mariathasan S, Turley SJ, Nickles D, Castiglioni A, Yuen K, Wang Y, et al. TGFβ attenuates tumour response to PD-L1 Blockade by contributing to exclusion of T cells. Nature. 2018;554:544–8.
34. Malta TM, Sokolov A, Gentles AJ, Burzykowski T, Poisson L, Weinstein JN et al. Machine learning identifies stemness features associated with oncogenic dedifferentiation. Cell. 2018; 173: 338 – 54.e15.
35. Mayakonda A, Lin DC, Assenov Y, Plass C, Koeffler HP. Maftools: efficient and comprehensive analysis of somatic variants in cancer. Genome Res. 2018;28:1747–56.
36. Gu Z, Eils R, Schlesner M. Complex heatmaps reveal patterns and correlations in multidimensional genomic data. Bioinformatics. 2016;32:2847–9.
37. Zhang H, Meltzer P, Davis S. RCircos: an R package for circos 2D track plots. BMC Bioinformatics. 2013;14:244.
38. Szklarczyk D, Gable AL, Lyon D, Junge A, Wyder S, Huerta-Cepas J, et al. STRING v11: protein-protein association networks with increased coverage, supporting functional discovery in genome-wide experimental datasets. Nucleic Acids Res. 2019;47:D607–13.
39. Shannon P, Markiel A, Ozier O, Baliga NS, Wang JT, Ramage D, et al. Cytoscape: a software environment for integrated models of biomolecular interaction networks. Genome Res. 2003;13:2498–504.

40. Xu Q, Xu H, Deng R, Li N, Mu R, Qi Z, et al. Landscape of prognostic m6A RNA methylation regulators in hepatocellular carcinoma to aid immunotherapy. Front Cell Dev Biol. 2021;9:669145.
41. Shen X, Hu B, Xu J, Qin W, Fu Y, Wang S, et al. The m6A methylation landscape stratifies hepatocellular carcinoma into 3 subtypes with distinct metabolic characteristics. Cancer Biol Med. 2020;17:937–52.
42. Wilkerson MD, Hayes DN. ConsensusClusterPlus: a class discovery tool with confidence assessments and item tracking. Bioinformatics. 2010;26:1572–3.
43. Hänzelmann S, Castelo R, Guinney J. GSVA: gene set variation analysis for microarray and RNA-seq data. BMC Bioinformatics. 2013;14:7.
44. Korotkevich G, Sukhov V, Budin N, Shpak B, Artyomov MN, Sergushichev A. Fast gene set enrichment analysis. BioRxiv. 2016: 060012.
45. Charoentong P, Finotello F, Angelova M, Mayer C, Efremova M, Rieder D, et al. Pan-cancer Immunogenomic analyses reveal Genotype-Immunophenotype relationships and predictors of response to checkpoint Blockade. Cell Rep. 2017;18:248–62.
46. Jiang P, Gu S, Pan D, Fu J, Sahu A, Hu X, et al. Signatures of T cell dysfunction and exclusion predict cancer immunotherapy response. Nat Med. 2018;24:1550–8.
47. Yoshihara K, Shahmoradgoli M, Martínez E, Vegesna R, Kim H, Torres-Garcia W, et al. Inferring tumour purity and stromal and immune cell admixture from expression data. Nat Commun. 2013;4:2612.
48. Benjamini Y, Hochberg Y. Controlling the false discovery rate: a practical and powerful approach to multiple testing. J Roy Stat Soc: Ser B (Methodol). 1995;57:289–300.
49. Yu G, Wang LG, Han Y, He QY. ClusterProfiler: an R package for comparing biological themes among gene clusters. Omics. 2012;16:284–7.
50. Friedman J, Hastie T, Tibshirani R. Regularization paths for generalized linear models via coordinate descent. J Stat Softw. 2010;33:1–22.
51. Simon N, Friedman J, Hastie T, Tibshirani R. Regularization paths for cox's proportional hazards model via coordinate descent. J Stat Softw. 2011;39:1–13.
52. Meng Q, Lu YX, Ruan DY, Yu K, Chen YX, Xiao M, et al. DNA methylation regulator-mediated modification patterns and tumor microenvironment characterization in gastric cancer. Mol Ther Nucleic Acids. 2021;24:695–710.
53. Jardim DL, Goodman A, de Melo Gagliato D, Kurzrock R. The challenges of tumor mutational burden as an immunotherapy biomarker. Cancer Cell. 2021;39:154–73.
54. Dudley JC, Lin MT, Le DT, Eshleman JR. Microsatellite instability as a biomarker for PD-1 Blockade. Clin Cancer Res. 2016;22:813–20.
55. Li X, Ma S, Deng Y, Yi P, Yu J. Targeting the RNA m(6)A modification for cancer immunotherapy. Mol Cancer. 2022;21:76.
56. Alarcón CR, Goodarzi H, Lee H, Liu X, Tavazoie S, Tavazoie SF. HNRNPA2B1 is a mediator of m(6)A-Dependent nuclear RNA processing events. Cell. 2015;162:1299–308.

Publisher's note